

Chirality-dependent spin-transfer torque and current-induced spin rotation in helimagnetsV. V. Ustinov^{1,2,*} and I. A. Yasyulevich¹¹*Institute of Metal Physics, 620108 Ekaterinburg, Russian Federation*²*Ural Federal University, 620002 Ekaterinburg, Russian Federation*

(Received 3 February 2022; revised 8 July 2022; accepted 28 July 2022; published 11 August 2022)

We have built a theory of the spin-transfer torque (STT) effect in a conductive chiral helical magnet (CHM). It is shown that the STT effect induced by a spin current flowing through CHM leads to the rotation of the CHM magnetization spiral around its axis. The frequency of such rotation of the CHM magnetization is found. The former is expressed in terms of the parameters of the quantum-exchange Hamiltonian that specifies helical magnetic ordering in a conductive crystal. We have showcased that both the direction of rotation of the CHM magnetization and the direction of changes in the shape of the magnetic spiral are determined by the electron flow direction and the chirality of the magnet. The theory developed accounts for the generation of an electromagnetic field when rotating the magnetic spiral in the CHM subjected to an electric current flowing through the helimagnet.

DOI: [10.1103/PhysRevB.106.064417](https://doi.org/10.1103/PhysRevB.106.064417)**I. INTRODUCTION**

Spin-transport phenomena in conductive solids are today the subject of numerous research activities in spintronics. The theory of the magnetic dynamics of conductive chiral helimagnets (CHMs) under conditions of electric and spin currents flowing through them underlies the subject of this paper.

This paper aims to find the conditions under which the magnetic system of the conductive CHM, termed “helicoid” hereafter for brevity, rotates as a whole when direct electric current and related spin-moment flux pass through the helimagnet. To date in the literature, there are quite a few publications on the motion of a magnetic subsystem of conductive ferromagnetic materials under an electric current. Slonczewski [1] and Berger [2–4] were the first to initiate such investigations. When a spin-polarized electric current flows through the material, a spin moment of moving electrons is transferred to the magnetically ordered system of the material. This happens due to the exchange interaction between the traveling electrons and electrons localized at the crystal lattice sites, and due to the fulfillment of the conservation law for spin. As a consequence, a torque acting on the ferromagnet magnetization emerges. Such a process is called “spin-transfer torque” (STT). STT induced by the electric current can lead to the motion of domain walls, magnetization reversal of magnetic systems, generation of spin waves, and other fascinating effects.

In Refs. [5–9], an experiment was conducted on a system consisting of a fixed ferromagnetic layer, a nonmagnetic layer, and a free ferromagnetic layer. Its essence lies in the following: an electric current flowing through the first layer becomes spin polarized and can induce stationary precessional mo-

tion of the magnetization of the free ferromagnetic layer. Such a system, which gained the name of the spin-torque nano-oscillator, can be used as a generator of high-frequency electromagnetic waves ranging from GHz to THz. The generation of electromagnetic radiation due to the STT effect is possible not only in multilayer spintronic devices, but also in bulk magnets, for example, in ferromagnets possessing regions with an inhomogeneous distribution of magnetization [10]. It was demonstrated in Ref. [11] that when exposed to a spin-polarized current, the domain walls (DW) of a ferromagnet cause a change in the orientation of the conduction electron spins. In response to this action, the electrons create an equal but counterdirectional torque acting on DW. As a result, rotation and/or linear DW motion can occur.

In recent years, some papers have reported on the possible manipulation of the magnetization of helimagnets through the STT effect. The publications of Refs. [12–15] research the influence of an electric current on the magnetization motion of CHMs using numerical simulation of the solution to the Landau-Lifshitz-Gilbert (LLG) equation supplemented by phenomenological “adiabatic” and “nonadiabatic” terms describing the STT effect. When the current passes through CHMs, the spin spiral was found to shift as a whole, which is equivalent to the harmonic rotation of the spiral around its axis. It is shown that the helicoid displacement velocity is linearly dependent on the applied electric current. In this case, a transition arises from spin ordering of the “simple helix” type to “conical helix” ordering, with the angle of deviation from the simple helix increasing, as the current goes up. The paper of Ref. [16] explores the dynamics of a spiral spin-density wave in an easy-plane anisotropy CHM affected by an electric current, having combined calculations from first principles and the semiclassical linear response theory. Similarly to phenomenological calculations, it was found that the torque driven by the current causes the rotation of the spin spiral as a whole. In the most recent years, experimentally induced

*ustinov@imp.uran.ru

electric current motion of a spin spiral has been discovered and reflected in Refs. [17,18].

The aim of the present paper is to build a consistent theory of the STT effect in chiral conductive helimagnets. Its results should be (i) analytical formulas relating the frequency of the current-induced rotation of the magnetic spiral of a helimagnet and the characteristics of quantum-exchange interactions responsible for the formation of helimagnetic ordering in crystals; (ii) explicit expressions describing a change in the characteristics of a spin spiral due to a flowing current, including the conicity angle of the spiral and its spatial period.

Here, we consider the phenomena of spin-transfer torque in chiral helimagnets. In doing so, we take into account the essential circumstance that the motion of conduction electrons in an inhomogeneously magnetized system as a chiral helimagnet occurs in a substantially inhomogeneous magnetic field of the quantum-exchange origin. This leads to additional forces assigned by the gradients of exchange-field components, which act on the electron spin. As a consequence, they can noticeably affect the picture of the motion of the spin carriers. The existence of such effects was first demonstrated in the famous experiments of Stern-Gerlach [19]. In Ref. [20], the authors of the present paper showcased that the existence of the above-mentioned forces give rise to an augment in electrical resistance of chiral helimagnets. The paper of Ref. [21] describes the electrical magnetochiral and kinetic magnetoelectric effects induced by chiral exchange fields in CHMs. To analyze the influence of the STT effect on the dynamics of chiral magnetization in CHMs, we further exploit the quantum theory for spin transport of conduction electrons, developed in Refs. [20,21]. The equations of motion for the magnetization of conduction electrons, formulated in Refs. [20,21], will be supplemented by both equations describing the motion of the magnetization of localized electrons and Maxwell's equations describing the electromagnetic field generated by the rotating magnetization.

II. BASIC EQUATIONS

To outline the spin dynamics of helimagnets, we resort to the well-known model that offers the existence of “itinerant” and “localized” carriers of electric charge and spin in a conductive magnetically ordered crystal. Conduction electrons populating the overlapping exterior s shells of the atoms (further called s electrons) are as a rule responsible for the transport properties of conductive magnets. Localized electrons residing in the inner d (or f) shells of the crystal atoms and therefore called d electrons govern magnetic ordering in a crystal.

It is well known that the helical magnetic order in a system of localized electrons of inversion-center-free crystals can be described accounting for the direct Heisenberg exchange interaction and the Dzyaloshinskii-Moriya interaction between localized electrons, as well as magnetocrystalline anisotropy. Spin interactions in the system of localized electrons can be effectively covered in the language of spin operators. Let us introduce the spin operator $\hat{\mathbf{S}}_n$ for the electrons localized at crystal lattice sites with numbers n . We designate the spin operator for the itinerant electrons as a lowercase letter $\hat{\mathbf{s}}$. For illustrating the interaction between the itinerant and localized

electrons, we apply the well-known s - d exchange model. The spin Hamiltonian of the system subjected to the external field \mathbf{B} can be written in the form

$$\begin{aligned} \hat{H} = & -(1/2) \left\{ \sum_{n,m} I_{nm} \hat{\mathbf{S}}_n \cdot \hat{\mathbf{S}}_m + \sum_{n,m} \mathcal{D}_{nm} \cdot [\hat{\mathbf{S}}_n \times \hat{\mathbf{S}}_m] \right. \\ & \left. - \mathcal{K} \sum_n (\hat{\mathbf{S}}_n \cdot \mathbf{e}_z)^2 \right\} + g\mu_B \left(\sum_n \hat{\mathbf{S}}_n + \sum_i \hat{\mathbf{s}}_i \right) \cdot \mathbf{B} \\ & - \sum_{i,n} I(\mathbf{r}_i - \mathbf{r}_n) \hat{\mathbf{s}}_i \cdot \hat{\mathbf{S}}_n. \end{aligned} \quad (1)$$

Here, I_{nm} are the values of the Heisenberg exchange interaction of spins localized at crystal lattice sites with numbers n and m , vector quantities \mathcal{D}_{nm} characterize the anisotropic Dzyaloshinskii-Moriya interaction between spins $\hat{\mathbf{S}}_n$ and $\hat{\mathbf{S}}_m$, $I(\mathbf{r}_i - \mathbf{r}_n)$ is the integral of the s - d exchange interaction of a conduction electron with a coordinate \mathbf{r}_i and electrons localized at a lattice site \mathbf{r}_n , \mathcal{K} is the single-ion anisotropy constant, g is the g factor of the electron, and μ_B is the Bohr magneton, \mathbf{e}_z is the unit vector pointing along the preferred direction in a magnetically uniaxial crystal, which in this study was assumed to be aligned with the axis OZ .

Let us go over from the quantum-mechanical description of the system in the language of spin operators $\hat{\mathbf{S}}_n$ to the classical one by formally replacing the spin operators in the Hamiltonian \hat{H} by the classical vectors $\mathbf{S}_n = -(V/g\mu_B)\mathbf{M}(\mathbf{r}_n)$, where $\mathbf{M}(\mathbf{r}_n)$ is the magnetization of localized electrons at the lattice sites \mathbf{r}_n , V is the volume of the Wigner-Seitz cell of a crystal. The magnetization $\mathbf{M}(\mathbf{r})$ is assumed to be a continuously varying quantity in coordinate space. Consequently, from Eq. (1) we arrive at the following representation for the magnetic energy density of the crystal in terms of the magnetizations $\mathbf{M}(\mathbf{r})$ and $\mathbf{m}(\mathbf{r})$ for localized electrons and conduction electrons, respectively:

$$\begin{aligned} \mathcal{F} = & -(1/2) \{ C \mathbf{M}^2 + \mathbf{M} \cdot \nabla \cdot \vec{\mathcal{A}} \cdot \nabla \mathbf{M} - 2\mathbf{M} \cdot [\vec{\mathcal{D}} \cdot \nabla \times \mathbf{M}] \\ & - \mathcal{B}(\mathbf{M} \cdot \mathbf{e}_z)^2 \} - (\mathbf{M} + \mathbf{m}) \cdot \mathbf{B} - \Lambda \mathbf{M} \cdot \mathbf{m}. \end{aligned} \quad (2)$$

Here, $C = (V/g^2\mu_B^2) \sum_m I_{0m}$, $\vec{\mathcal{A}} = (V/2g^2\mu_B^2) \sum_m I_{0m} \delta \mathbf{r}_{m0} \otimes \delta \mathbf{r}_{m0}$, $\vec{\mathcal{D}} = (V/2g^2\mu_B^2) \sum_m \mathcal{D}_{0m} \otimes \delta \mathbf{r}_{m0}$, $\mathcal{B} = (V/g^2\mu_B^2) \mathcal{K}$, and $\Lambda = (1/g^2\mu_B^2) \int I(\mathbf{r}) d^3\mathbf{r}$.

The sign \otimes is used here to denote the tensor product of vectors, so that the quantities $\vec{\mathcal{A}}$ and $\vec{\mathcal{D}}$ in Eq. (2) are the second-rank tensors. Restricting ourselves to considering crystals of cubic symmetry, we represent the tensors $\vec{\mathcal{A}}$ and $\vec{\mathcal{D}}$ in the form $\vec{\mathcal{A}} = \mathcal{A} \vec{\mathcal{E}}$ and $\vec{\mathcal{D}} = \mathcal{D} \vec{\mathcal{E}}$, where \mathcal{A} and \mathcal{D} are constants, and $\vec{\mathcal{E}}$ is the unit second-rank tensor. The quantity \mathcal{A} is referred to as “exchange stiffness,” while the special term “spiralization” can be utilized for verbal identification of the quantity \mathcal{D} .

Calculating the free energy $F = \int \mathcal{F} d^3\mathbf{r}$ of the crystal followed by the variational derivatives of F over the variables \mathbf{m} and \mathbf{M} , we find the effective magnetic fields $\mathbf{B}_m^{(\text{eff})} = -\delta F / \delta \mathbf{m}$ and $\mathbf{B}_M^{(\text{eff})} = -\delta F / \delta \mathbf{M}$ acting on the magnetization \mathbf{m} and \mathbf{M} :

$$\mathbf{B}_m^{(\text{eff})} = \mathbf{B} + \Lambda \mathbf{M}, \quad (3)$$

$$\begin{aligned} \mathbf{B}_M^{(\text{eff})} = & \mathbf{B} + \mathcal{A} \Delta \mathbf{M} - \mathcal{B}(\mathbf{M} \cdot \mathbf{e}_z) \mathbf{e}_z + C \mathbf{M} - 2\mathcal{D}[\nabla \times \mathbf{M}] \\ & + \Lambda \mathbf{m}. \end{aligned} \quad (4)$$

The dynamics of the magnetization \mathbf{m} can be interpreted by the Bloch-Torrey equation to take into account the spin-diffusion currents carried by conduction electrons:

$$\partial\mathbf{m}/\partial t + \gamma[\mathbf{m} \times \mathbf{B}_m^{\text{eff}}] + \nabla \cdot \tilde{\mathbf{J}}_m + \delta\mathbf{m}/\tau_S = 0. \quad (5)$$

The second term on the left-hand side of Eq. (5) describes the precessional motion in the effective magnetic field $\mathbf{B}_m^{\text{eff}}$. The third term that underlies changes in \mathbf{m} under spin currents contains a quantity $\tilde{\mathbf{J}}_m$. The latter is the spin-current tensor of the itinerant electrons. The rigorous derivation of the equation of motion for the spin-current tensor $\tilde{\mathbf{J}}_m$ has been published elsewhere [20,21]. The tensor $\tilde{\mathbf{J}}_m$ can be written as

$$\tilde{\mathbf{J}}_m = -D\nabla \otimes \delta\mathbf{m} + \mathbf{w} \otimes \mathbf{m}. \quad (6)$$

The first term on the right-hand side of Eq. (6) describes the diffusion spin current arising in the inhomogeneously magnetized system of conduction electrons. Here, D is the electron diffusion coefficient, and $\delta\mathbf{m} \equiv \mathbf{m} - \chi\mathbf{B}_m^{\text{eff}}$ is the deviation of the electron magnetization \mathbf{m} from its local equilibrium value $\chi\mathbf{B}_m^{\text{eff}}$, where the quantity χ is the Pauli susceptibility of a conduction electron gas. The second summand on the right-hand side of Eq. (6) is responsible for the spatial transfer of the spin moment by a flow of electrons moving with a drift velocity \mathbf{w} . The latter regulates the value of the density of the electric current \mathbf{j} passing through the system: $\mathbf{j} = Ne\mathbf{w}$. Here, N is the carrier concentration and e is the charge of an electron. Expression (6) for the spin-electron current is valid when the cyclotron frequency and the Larmor frequency of conduction electrons are negligibly small compared to $1/\tau$, where τ is the momentum relaxation time of electrons.

The last term on the left-hand side of Eq. (5) operates the spin-lattice relaxation of the magnetization \mathbf{m} to its local-equilibrium value $\chi\mathbf{B}_m^{\text{eff}}$ and includes the quantity τ_S being the spin-lattice relaxation time of the itinerant electrons.

To gain an insight into the dynamics of magnetization \mathbf{M} , we utilize the LLG equation:

$$\partial\mathbf{M}/\partial t + \gamma[\mathbf{M} \times \mathbf{B}_M^{\text{eff}}] + (\alpha/M)[\partial\mathbf{M}/\partial t \times \mathbf{M}] = 0, \quad (7)$$

where γ is the gyromagnetic ratio, α is the Gilbert damping constant, $M = |\mathbf{M}|$. The use of the LLG equation ensures that the length M of magnetization vector \mathbf{M} will be unconditionally conserved.

Plugging all the terms of expression (4) for the effective magnetic field $\mathbf{B}_M^{\text{eff}}$ into the LLG Eq. (7), we can write the equation in the following form:

$$\begin{aligned} \partial\mathbf{M}/\partial t + \gamma[\mathbf{M} \times (\mathbf{B} + \mathbf{B}_B)] + \nabla \cdot \tilde{\mathbf{J}}_M \\ + (\alpha/M)[\partial\mathbf{M}/\partial t \times \mathbf{M}] + \mathbf{T} = 0. \end{aligned} \quad (8)$$

The second term $\gamma[\mathbf{M} \times (\mathbf{B} + \mathbf{B}_B)]$ on the left-hand side of Eq. (8) is obtained as a result of substitution of the first three summands from expression (4) for $\mathbf{B}_M^{\text{eff}}$ into Eq. (7). It describes the precession of the magnetization \mathbf{M} under the field \mathbf{B} and the uniaxial anisotropy field $\mathbf{B}_B = \mathcal{B}(\mathbf{M} \cdot \mathbf{e}_z)\mathbf{e}_z$.

The third term $\nabla \cdot \tilde{\mathbf{J}}_M$ on the left-hand side of Eq. (8) is derived after substitution of fourth and fifth terms from expression (4) into Eq. (7). Using easily proven relations of tensor algebra, such as $[\mathbf{M} \times \Delta\mathbf{M}] = -\nabla \cdot [(\nabla \otimes \mathbf{M}) \times \mathbf{M}]$ and $[\mathbf{M} \times [\nabla \times \mathbf{M}]] = -\nabla \cdot \mathbf{M} \otimes \mathbf{M}$, we have come up with

$\nabla \cdot \tilde{\mathbf{J}}_M$, where we have introduced the exchange spin-current tensor

$$\tilde{\mathbf{J}}_M = -\gamma\mathcal{A}[(\nabla \otimes \mathbf{M}) \times \mathbf{M}] + 2\gamma\mathcal{D}\mathbf{M} \otimes \mathbf{M}. \quad (9)$$

It should be separately emphasized that the exchange spin current $\tilde{\mathbf{J}}_M$ introduced above appears in the system of localized electrons solely due to their mutual exchange interactions rather than due to the ‘‘transport’’ spin transfer in coordinate space, as in the case of the spin current $\tilde{\mathbf{J}}_m$ in the system of noninteracting conduction electrons.

The last term \mathbf{T} on the left-hand side of Eq. (8) is a result of substitution of the sixth term from expression (4) into Eq. (7). It is dictated by the equation

$$\mathbf{T} = \gamma\Delta[\mathbf{M} \times \mathbf{m}], \quad (10)$$

and reflects the STT effect between the systems of itinerant and localized electrons. The vector \mathbf{T} has the meaning of a torque acting on the magnetization \mathbf{M} of the localized electrons from the conduction electrons with the magnetization \mathbf{m} .

Since the change in time and space of the total magnetization $\mathbf{M} + \mathbf{m}$ of the system generates an inhomogeneous alternating electromagnetic field, in the general case, the set of coupled equations of motion (5) and (8) should be solved jointly with Maxwell’s equations for the strengths of the magnetic \mathbf{H} and electric \mathbf{E} fields:

$$\begin{aligned} [\nabla \times \mathbf{H}] &= (4\pi/c)\mathbf{j} + (1/c)\partial\mathbf{E}/\partial t, \\ [\nabla \times \mathbf{E}] &= -(1/c)\partial\mathbf{B}/\partial t. \end{aligned} \quad (11)$$

Knowing the strength of the $\mathbf{H} = \mathbf{B} - 4\pi(\mathbf{M} + \mathbf{m})$ and \mathbf{E} fields, we can evaluate the Umov-Poynting vector:

$$\mathbf{U} = (c/4\pi)[\mathbf{E} \times \mathbf{H}]. \quad (12)$$

This vector defines the energy flux density vector of the electromagnetic field excited in the helimagnet when the inhomogeneous magnetization varies with time.

III. EQUILIBRIUM STATE OF A HELIMAGNET

Let us look into the case when a constant external magnetic field \mathbf{B}_ℓ is directed along the OZ axis.

In the absence of an electric current, the \mathbf{M} and \mathbf{m} magnetizations in the equilibrium state are time independent and are functions of only the z coordinate. Equilibrium magnetization of the itinerant electrons is equal to $\mathbf{m}_0 = \chi(\mathbf{B}_\ell + \Delta\mathbf{M}_0)$. An equilibrium distribution $\mathbf{M}_0(z)$ is defined as an extremal of the energy functional F to meet the condition $|\mathbf{M}_0(z)| = M$ and to provide the minimum value of the functional F . To find the extremes of the functional F with the additional requirement $\mathbf{M}^2 - M^2 = 0$, the set of Euler-Poisson equations needs to be solved.

It can be shown that the solution to the Euler-Poisson equation that includes an energy density (2) is a magnetic helicoid, $\mathbf{M}(z) = \mathbf{M}_\ell + \mathbf{M}_t(z)$. The longitudinal (with respect to the OZ axis) magnetization component \mathbf{M}_ℓ of this helicoid is z -coordinate independent. The transverse component \mathbf{M}_t alters harmoniously abiding by the law $\mathbf{M}_t(z) = M_t(\mathbf{e}_x \cos q_z z + \mathbf{e}_y \sin q_z z)$ with growth of z . In this case,

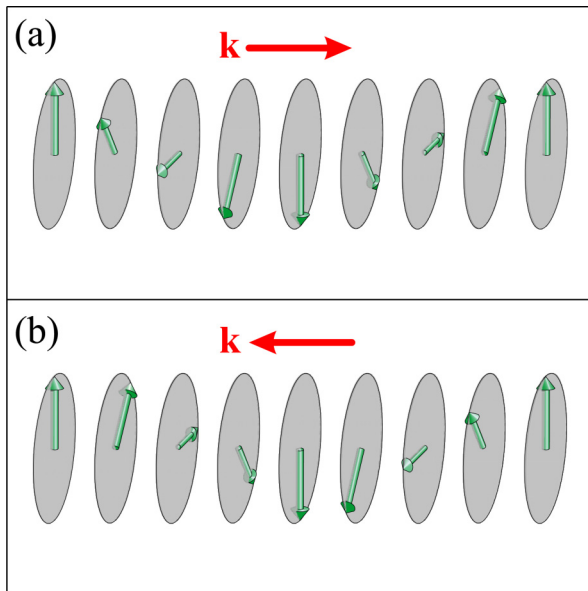


FIG. 1. Scheme of the spatial configuration of a simple magnetic spiral of a helimagnet with a chirality vector \mathbf{k} in the absence of a magnetic field: (a) a right-handed spiral, chirality is $K = +1$; (b) a left-handed spiral. Chirality is $K = -1$.

the length M_t of the vector $\mathbf{M}_t(z)$ is conserved, and its direction changes in space with a period $2\pi/q$, where $q = |\mathbf{q}|$ is the wave number of the helicoid with the wave vector $\mathbf{q} = [\mathbf{M}_t \times \partial \mathbf{M}_t / \partial z] / M_t^2$, and $q_z = \mathbf{q} \cdot \mathbf{e}_z$. It is convenient to write down the value of the z component of the wave vector \mathbf{q} as $q_z = Kq$, where K is the spin spiral chirality that takes the values of $K = \pm 1$. Hereinafter in this paper, we exploit the unit chirality vector $\mathbf{k} = \mathbf{q}/q = K\mathbf{e}_z$ to characterize the chiral helicoid, apart from the scalar quantity K .

When the wave number and the chirality are $q = q_0 \equiv |\mathcal{D}|/\mathcal{A}$ and $K = \text{sgn}\mathcal{D}$, respectively, the value of the magnetic spiral energy in equilibrium is minimum. For equilibrium, we get a relationship between $\mathbf{M}_{0\ell}$ and \mathbf{B}_ℓ as

$$\mathbf{M}_{0\ell} = \frac{1 + \chi \Lambda}{\mathcal{B} + \mathcal{D}^2/\mathcal{A}} \mathbf{B}_\ell. \quad (13)$$

In the absence of a magnetic field, a magnetic structure of the ‘‘simple spiral’’ type emerges. Only the transverse components of the magnetization \mathbf{M}_t are nonzero in this structure. Scheme of the magnetic structure of a simple spiral is depicted in Fig. 1.

By applying external magnetic field along the axis of magnetic spiral, one can transform the latter into a magnetic structure of the ‘‘conical spiral’’ type. In such a magnetic structure, both the transverse components of the magnetization \mathbf{M}_t and the longitudinal component of the magnetization \mathbf{M}_ℓ are nonzero. Let us introduce the angle θ of the magnetic spiral conicity to characterize the deviation of the vector \mathbf{M} from the XY plane through the ratio $\sin \theta = (\mathbf{M}_\ell \cdot \mathbf{e}_z)/M$. Then, for the equilibrium helicoid, we can claim that $\sin \theta_0 = B_z/B_F$, where $B_z = \mathbf{B} \cdot \mathbf{e}_z$, and $B_F = M(\mathcal{B} + \mathcal{D}^2/\mathcal{A})/(1 + \chi \Lambda)$. In equilibrium, the anisotropy type chosen above assigns no direction of the transverse magnetization. Upon reaching the value B_F , the magnetic field B makes the conical spiral undergo a phase

transition to the ‘‘ferromagnetic’’ state with $|\mathbf{M}_\ell| = M$ and $\mathbf{M}_t(z) = 0$. The characteristic conical spiral configuration of magnetic moments is illustrated in Fig. 2.

IV. MAGNETIC DYNAMICS OF A HELIMAGNET

Let us explore the dynamics of the \mathbf{M} and \mathbf{m} magnetizations of a helimagnet under a constant electric density current \mathbf{j}_ℓ flowing along the magnetic spiral axis. We can show that a set of coupled equations for \mathbf{M} , \mathbf{m} , and \mathbf{B} has a solution that describes the harmonic rotation of the magnetic spiral around its axis with a \mathbf{j}_ℓ -dependent frequency ω . The solutions for \mathbf{M} , \mathbf{m} , and \mathbf{B} should be sought under the assumption that the lengths of the vectors \mathbf{M}_t , \mathbf{m}_t , and \mathbf{B}_t are coordinates- and time independent, whereas their directions obey the law $\sim [\mathbf{e}_x \cos(q_z z - \omega t) + \mathbf{e}_y \sin(q_z z - \omega t)]$.

When solving the Maxwell equations (11), we suppose a relationship between the density of the current \mathbf{j} and the electric field \mathbf{E} through Ohm’s law $\mathbf{j} = \sigma \mathbf{E}$, where σ is the specific electrical conductivity of the magnet. From Eqs. (11) it follows that the transverse components of the magnetic induction \mathbf{B} and the total magnetization $\mathcal{M} = \mathbf{M} + \mathbf{m}$ of the helimagnet are related by the equation $\mathbf{B}_t = \eta_{\parallel} \mathcal{M}_t + \eta_{\perp} [\mathbf{e}_z \times \mathcal{M}_t]$. Neglecting the bias currents, we can express the quantities η_{\parallel} and η_{\perp} as $\eta_{\parallel} = 4\pi/(1 + \xi^2)$ and $\eta_{\perp} = 4\pi\xi/(1 + \xi^2)$, respectively, where $\xi = \omega/\Omega_\sigma$, $\Omega_\sigma = q^2 c^2/4\pi\sigma$. Next, we assume that $\omega \ll \Omega_\sigma$ in the entire range of frequencies studied. Then, $\xi \ll 1$, $\eta_{\parallel} \approx 4\pi$, and $\eta_{\perp} \approx 4\pi\xi$.

Solving the set of Eqs. (5)–(10) can be significantly facilitated by applying a small parameter χ called the Pauli susceptibility that is smaller than unity by several orders of magnitude. Estimates of χ for some specific metallic helimagnets will be given below in Sec. VI. Taking into account the discussed parameter ranges, it is estimated that $\chi \sim 10^{-7} - 10^{-6}$.

The magnitude of the s - d exchange interaction is characterized by a dimensionless parameter Λ . For typical conductive magnets, the value of Λ is much greater than unity. Below, in Sec. VI we will present estimates of Λ for some metallic helimagnets. Considering the discussed parameter values, one can expect that $\Lambda \sim 10^3 - 10^4$. Taking into account the discussed χ and Λ parameter ranges, it is estimated that the product of the small $\chi \ll 1$ and large $\Lambda \gg 1$ parameters is small in comparison with unity: $\chi \Lambda \ll 1$.

The smallness of the parameters χ , Λ^{-1} , $\chi \Lambda$, and ξ brings Eq. (5) to the following set of equations for $\delta \mathbf{m}_t$ and $\delta \mathbf{m}_\ell$:

$$(\omega - \mathbf{q} \cdot \mathbf{w} + \Omega_z + \Omega_H \sin \theta) [\delta \mathbf{m}_t \times \mathbf{e}_z] + (\nu_S + \nu_D) \delta \mathbf{m}_t + \gamma \Lambda [\delta \mathbf{m}_\ell \times \mathbf{M}_t] = \chi (\mathbf{q} \cdot \mathbf{w} - \omega) [(\mathbf{B}_t + \Lambda \mathbf{M}_t) \times \mathbf{e}_z], \quad (14)$$

$$\nu_S \delta \mathbf{m}_\ell + \gamma [\delta \mathbf{m}_t \times (\mathbf{B}_t + \Lambda \mathbf{M}_t)] = 0. \quad (15)$$

Equation (14) includes the following designations: $\Omega_z = \gamma B_z$ is the frequency of precession in the field B_z , $\Omega_H = \gamma \Lambda M$ is the frequency of precession in the exchange field ΛM , $\nu_S = 1/\tau_S$ is the spin-lattice relaxation rate, $\nu_D = q^2 D$ is the spin-diffusion relaxation rate. The rates ν_S and ν_D have the units of frequency. The solution to the set of equations (14) and (15)

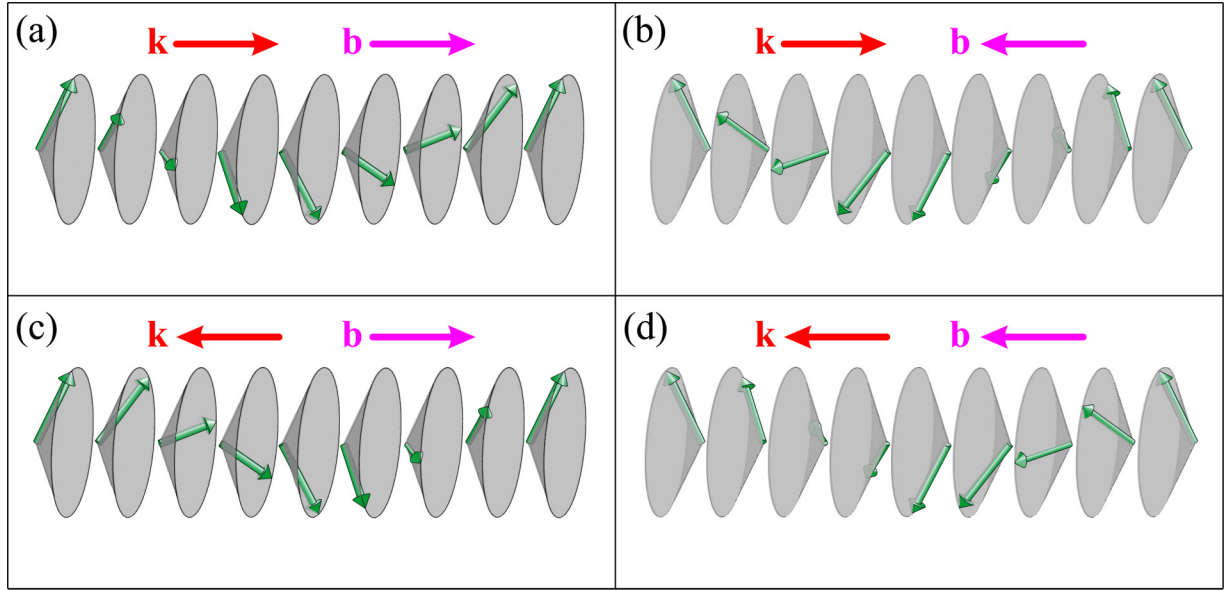


FIG. 2. Stable conical magnetic spiral formed in a helimagnet subjected to an external magnetic field, the direction of which is given by the unit vector $\mathbf{b} = \mathbf{B}_\ell/|B_\ell|$: (a) right-handed spiral, \mathbf{b} is parallel to \mathbf{k} ; (b) right-handed spiral, \mathbf{b} is antiparallel to \mathbf{k} ; (c) left-handed spiral, \mathbf{b} is antiparallel to \mathbf{k} ; and (d) left-handed spiral, \mathbf{b} is parallel to \mathbf{k} .

can be represented as

$$\begin{aligned} \delta \mathbf{m}_\ell &= -(\gamma/v_S)\chi_\perp(\mathbf{B}_t + \Lambda \mathbf{M}_t)^2 \mathbf{e}_z, \\ \delta \mathbf{m}_t &= \chi_\parallel(\mathbf{B}_t + \Lambda \mathbf{M}_t) + \chi_\perp[(\mathbf{B}_t + \Lambda \mathbf{M}_t) \times \mathbf{e}_z], \end{aligned} \quad (16)$$

where the χ_\perp and χ_\parallel components of the tensor of the transverse magnetic permeability are defined as

$$\chi_\perp = \chi(\mathbf{q} \cdot \mathbf{w} - \omega)/v, \quad (17)$$

$$\chi_\parallel = \chi(\mathbf{q} \cdot \mathbf{w} - \omega)(\omega + \Omega_z + \Omega_H \sin \theta - \mathbf{q} \cdot \mathbf{w})/v(v_S + v_D), \quad (18)$$

where $v = v_S + v_D + (\Omega_H^2/v_S) \cos^2 \theta + (\omega + \Omega_z + \Omega_H \times \sin \theta - \mathbf{q} \cdot \mathbf{w})^2/(v_S + v_D)$.

Plugging the expressions derived for $\delta \mathbf{m}_t$ and $\delta \mathbf{m}_\ell$ into Eq. (10) for \mathbf{T} , from the LLG Eq. (8) we obtain a closed set of equations for the longitudinal \mathbf{M}_ℓ and transverse \mathbf{M}_t components of the magnetization \mathbf{M} . The condition for the existence of the solution as a helical wave with a wave vector \mathbf{q} under the assumptions made above about the smallness of the $\chi \Lambda$ and ξ parameters can be written in the form of a set of two coupled equations:

$$(\alpha + \Omega_M/\Omega_\sigma)\omega - \chi_\perp \Lambda \Omega_H = 0, \quad (19)$$

$$\omega + \Omega_z - \Omega \sin \theta = 0. \quad (20)$$

Here, $\Omega_M = 4\pi\gamma M$, $\Omega_F = \gamma B_F$, $\Omega = \Omega_F + \Omega_M[1 - (1/4\pi)\mathcal{A}(q - q_0)^2]$.

The wave number q is computed from the condition of the minimum magnetic energy F . If the exchange stiffness \mathcal{A} is sufficiently large, so that the condition $\mathcal{A}q_0^2 > 1$ holds, then q acquires the form of $q = q_0(1 + 16\pi\xi^2/\mathcal{A}q_0^2)$. It is easy to see that the wavelength of the rotating helicoid is always somewhat less than that of a stationary magnetic spiral. By virtue of the fulfillment of the condition $\xi \ll 1$, the deviation of q

from the equilibrium value q_0 is small and can be neglected further on, with $q = q_0$ and $\Omega = \Omega_F + \Omega_M$.

Next, we assume that the magnitude of the drift velocity w of conduction electrons is small in comparison with the magnitude of qD . The condition $w/qD \ll 1$ allows one to omit the term $\mathbf{q} \cdot \mathbf{w}$ when calculating the value of v . Using Eq. (20), we can now represent the effective spin-relaxation rate v for conduction electrons in CHM as

$$\begin{aligned} v &= v_S + v_D + (\Omega_H^2/v_S) \cos^2 \theta \\ &+ [(\Omega + \Omega_H)^2/(v_S + v_D)] \sin^2 \theta, \end{aligned} \quad (21)$$

where the angle θ that defines the magnetic spiral conicity is equal to

$$\theta = \arcsin[(\omega + \Omega_z)/\Omega]. \quad (22)$$

Substituting the expression (17) for χ_\perp into Eq. (19), we come up with an implicit expression for the frequency ω :

$$\omega = \frac{\Gamma}{\alpha_{\text{eff}} + \Gamma}(\mathbf{q} \cdot \mathbf{w}), \quad (23)$$

where $\Gamma = \chi \Lambda \Omega_H/v$ is a dimensionless quantity characterizing the efficiency of the SST process in the helimagnet, and $\alpha_{\text{eff}} = \alpha + \beta$, where $\beta = \Omega_M/\Omega_\sigma$ is the parameter of damping of magnetic oscillations, caused by losses upon switching on the electromagnetic field.

It is explicitly seen from Eq. (23) that the linear motion of the conduction electrons moving in space with the drift velocity \mathbf{w} transforms into the rotational motion of the helimagnet magnetic spiral with the frequency ω .

It should be especially underscored that Eq. (23) also reflects the opposite effect: the rotation of the magnetic spiral of a helimagnet, caused by an external electromagnetic field with a frequency ω , can be converted into a constant electric current of conduction electrons with a drift velocity \mathbf{w} . This

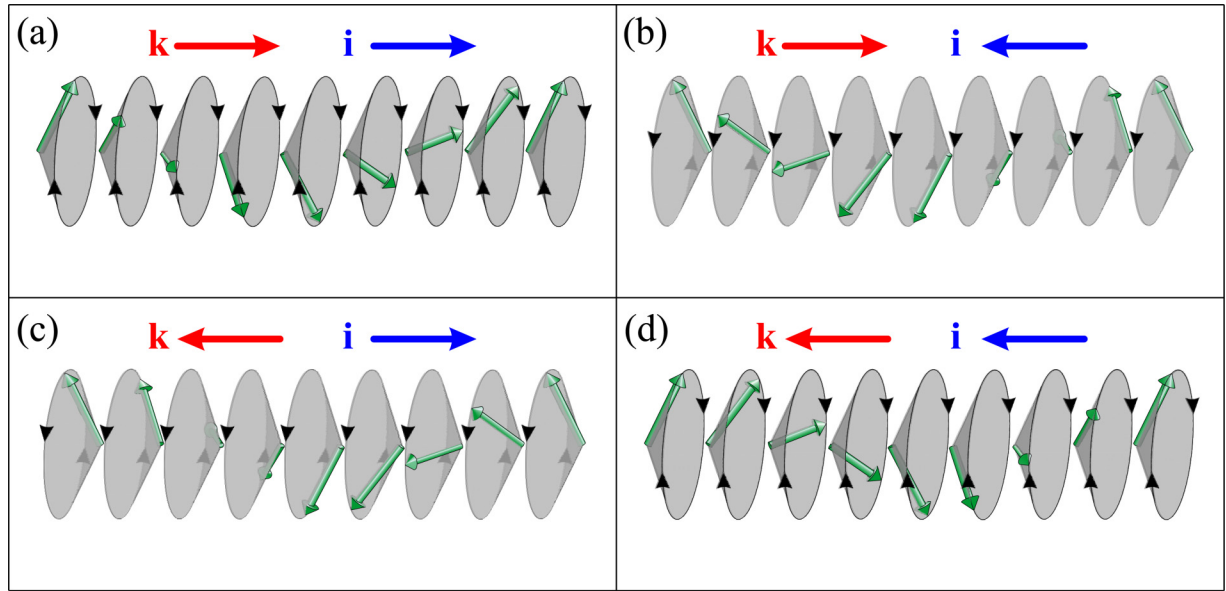


FIG. 3. Scheme of configurations of a conical magnetic spiral of a helimagnet with chirality \mathbf{k} , rotating under the action of an electron flow, the direction of which is given by a unit vector \mathbf{i} , in the absence of a magnetic field: (a) right-handed spiral, \mathbf{i} is parallel to \mathbf{k} ; (b) right-handed spiral, \mathbf{i} is antiparallel to \mathbf{k} ; (c) left-handed spiral, \mathbf{i} is antiparallel to \mathbf{k} ; and (d) left-handed spiral, \mathbf{i} is parallel to \mathbf{k} .

inverse effect can be described by the equation

$$\mathbf{w} = \left(1 + \frac{\alpha_{\text{eff}}}{\Gamma}\right) \frac{\omega}{q} \mathbf{k}. \quad (24)$$

It can be shown that the magnitude of the Umov-Poynting vector given by Eq. (12) within the approximations adopted previously can be represented as

$$U \approx 4\pi \frac{w^3 \mathcal{M}^2}{c^2} \left(\frac{\Gamma}{\alpha_{\text{eff}} + \Gamma}\right)^3 \cos^2 \theta. \quad (25)$$

Regardless of the magnet chirality, the radiation propagation direction coinciding with the direction of the Poynting vector is always parallel to the vector \mathbf{i} denoting the drift direction of the conduction electrons.

It is obvious that Eq. (20) implies the validity of the result (23) conditional upon the inequality $|\omega + \Omega_z| \leq \Omega$ is fulfilled. Here, the frequency Ω_z can take on both positive and negative values, depending on the direction of the constant magnetic field \mathbf{B}_ℓ . Let, for definiteness, the \mathbf{B}_ℓ and \mathbf{e}_z vectors be antiparallel, then $\Omega_z = -\Omega_L$, where $\Omega_L \geq 0$ is the Larmor frequency. Hence, the condition of applicability of Eq. (23) can be written as $-\Omega + \Omega_L \leq \omega \leq \Omega + \Omega_L$. If the \mathbf{B}_ℓ and \mathbf{e}_z vectors are parallel, the foregoing condition appears as $-\Omega - \Omega_L \leq \omega \leq \Omega - \Omega_L$ because $\Omega_z = +\Omega_L$. Thus, a direct electric current flowing in the helimagnet can induce the helimagnet's magnetic spiral rotation with a maximum possible frequency $\omega_{\text{max}} = \Omega + \Omega_L$.

V. MAGNETIC SPIRAL DYNAMICS WITHOUT AN EXTERNAL MAGNETIC FIELD

In the absence of external magnetic field $\Omega_L = 0$ and Eq. (23) holds true over the frequency range $-\Omega \leq \omega \leq \Omega$. In this case, the maximum possible value of the helicoid rotation frequency is determined by the value of $\Omega = \Omega_F + \Omega_M$. From Eqs. (22) and (23) it follows that an electric current flowing

along the axis of the magnetic spiral leads not only to its rotation but also to a change in its shape. When an external magnetic field is zero, the angle of conicity of the spiral rotated with a frequency ω , according to (22), is defined by the equation

$$\theta = \arcsin \frac{\omega}{\Omega}. \quad (26)$$

It clearly follows from Eq. (23) that due to the motion of electrons with a drift velocity \mathbf{w} , the sign of the helicoid rotation frequency is provided by the sign of the scalar product $(\mathbf{k} \cdot \mathbf{i})$. Here, $\mathbf{k} = \mathbf{q}/q$ is the unit vector of chirality, and $\mathbf{i} = \mathbf{w}/w$ is the unit vector that is directed along the motion of the itinerant electron flow. Figure 3 schematically depicts the dependence of the directions of the CHM magnetization spiral rotation and the spiral conicity on the mutual orientation of the chirality \mathbf{k} and flow \mathbf{i} vectors with no external magnetic field present.

Due to the fact that the ω -dependent angle θ [according to (26)] essentially affects the quantity ν determined by expression (21), relation (23) is an equation for finding ω as a function of the independent variable w . Accordingly, relation (24) is an equation for finding w as a function of the independent variable ω . Below, we will carry out a detailed analysis of the singularities of the solutions of these equations. For definiteness, consider the case when the \mathbf{i} and \mathbf{k} vectors are codirectional.

Let us introduce dimensionless parameters $\bar{v}_S = v_S/\Omega_H$, $\bar{v}_D = v_D/\Omega_H$, and $a = \alpha_{\text{eff}}/\chi\Lambda$, as well as dimensionless variables $\bar{w} = wq/\Omega$, $\bar{\omega} = \omega/\Omega$, and $\bar{v} = v/\Omega_H$. In the new notations, Eq. (23) appears as

$$\bar{w} = (1 + a\bar{v})\bar{\omega}. \quad (27)$$

In this equation, the variable \bar{w} is assigned in the semiaxis $\bar{w} \geq 0$, whereas the values of $\bar{\omega}$ are limited and lie in the range of $0 \leq \bar{\omega} \leq 1$.

Accounting for expression (21) for ν and relation (26), the quantity $\bar{\nu} = \nu/\Omega_H$ involved in Eq. (27) can be represented as

$$\bar{\nu} = \bar{\nu}_0 + (\bar{\nu}_1 - \bar{\nu}_0)\bar{\omega}^2, \quad (28)$$

where $\bar{\nu}_0 = \bar{\nu}_S + \bar{\nu}_D + 1/\bar{\nu}_S$ and $\bar{\nu}_1 = \bar{\nu}_S + \bar{\nu}_D + (1 + \Omega/\Omega_H)^2/(\bar{\nu}_S + \bar{\nu}_D)$. According to (28), the quantity $\bar{\nu}$ can be treated as a function of $\bar{\omega}$. With varying $\bar{\omega}$ from 0 to 1, the function $\bar{\nu}(\bar{\omega})$ changes from $\bar{\nu}_0$ to $\bar{\nu}_1$.

Substituting (28) into (27), we arrive at the following equation for finding $\bar{\omega}$ as a function of $\bar{\omega}$:

$$\bar{\omega} = \{1 + a[\bar{\nu}_0 + (\bar{\nu}_1 - \bar{\nu}_0)\bar{\omega}^2]\bar{\omega}\}. \quad (29)$$

It is easy to see that Eq. (29) gives an explicit form of the function $\bar{\omega}(\bar{\omega})$ that is inverse with respect to the sought-for function $\bar{\omega}(\bar{\omega})$. When $\bar{\omega}$ reaches the value $\bar{\omega} = 1$, the variable $\bar{\omega}$ according to (29) takes the value $\bar{\omega}_1 = 1 + a\bar{\nu}_1$. Depending on the ratio of the parameters $\bar{\nu}_0$ and $\bar{\nu}_1$, the function $\bar{\omega}(\bar{\omega})$ can behave along two fundamentally different scenarios.

Scenario I is implemented when the condition $\bar{\omega}'_{\bar{\omega}}(\bar{\omega} = 1) > 0$ is met. Here, $\bar{\omega}'_{\bar{\omega}}(\bar{\omega})$ is the derivative of the function $\bar{\omega}(\bar{\omega})$ over the variable $\bar{\omega}$. Under this condition, the function $\bar{\omega}(\bar{\omega})$ is a monotonically increasing one for the entire range $0 \leq \bar{\omega} \leq 1$. Taking into account the explicit form of $\bar{\omega}(\bar{\omega})$ (29), the condition for the implementation of scenario I can be written as

$$a(2\bar{\nu}_0 - 3\bar{\nu}_1) < 1. \quad (30)$$

When condition (30) is satisfied, the desired function $\bar{\omega}(\bar{\omega})$ is a monotonically increasing function of $\bar{\omega}$ defined in the interval $0 \leq \bar{\omega} \leq \bar{\omega}_1$. It possesses the values $\bar{\omega}(0) = 0$ and $\bar{\omega}(\bar{\omega}_1) = 1$ at the boundaries of the interval. For $\bar{\omega} > \bar{\omega}_1$, Eq. (29) has no solution in the range of admissible values of the function $\bar{\omega}(\bar{\omega})$.

Scenario II is brought about when the condition $\bar{\omega}'_{\bar{\omega}}(\bar{\omega} = 1) < 0$ holds. In this case, the function $\bar{\omega}(\bar{\omega})$ changes non-monotonically with growth of $\bar{\omega}$, reaching its maximum value $\bar{\omega}_2$ at a certain value of $\bar{\omega} = \bar{\omega}_2$. The value $\bar{\omega}_2$ can be deduced from the equation $\bar{\omega}'_{\bar{\omega}}(\bar{\omega}_2) = 0$. The explicit form of $\bar{\omega}(\bar{\omega})$ (29) makes it possible for the solution of this equation to be written explicitly:

$$\bar{\omega}_2 = \left[\frac{1 + a\bar{\nu}_0}{3a(\bar{\nu}_0 - \bar{\nu}_1)} \right]^{1/2}. \quad (31)$$

Accordingly, for the value $\bar{\omega}_2$, we get

$$\bar{\omega}_2 = \frac{2}{3}(1 + a\bar{\nu}_0)\bar{\omega}_2. \quad (32)$$

It is worth emphasizing that the condition for the validity of formulas (31) and (32) is the inequality

$$a(2\bar{\nu}_0 - 3\bar{\nu}_1) > 1. \quad (33)$$

In accordance with the foregoing, when condition (33) is satisfied, the function $\bar{\omega}(\bar{\omega})$ is multivalued and has two branches. The first branch $\bar{\omega}^{(1)}(\bar{\omega})$ exists in the region of $0 \leq \bar{\omega} \leq \bar{\omega}_2$. When changing $\bar{\omega}$ from 0 to $\bar{\omega}_2$, the function $\bar{\omega}^{(1)}(\bar{\omega})$ increases monotonically from $\bar{\omega}^{(1)}(0) = 0$ to $\bar{\omega}^{(1)}(\bar{\omega}_2) = \bar{\omega}_2$. The second branch $\bar{\omega}^{(2)}(\bar{\omega})$ is defined in the region of $\bar{\omega}_1 \leq \bar{\omega} \leq \bar{\omega}_2$. With the growth of $\bar{\omega}$ from $\bar{\omega}_1$ to $\bar{\omega}_2$, the function $\bar{\omega}^{(2)}(\bar{\omega})$ monotonically decays from $\bar{\omega}^{(2)}(\bar{\omega}_1) = 1$ to $\bar{\omega}^{(2)}(\bar{\omega}_2) = \bar{\omega}_2$. In the region of $\bar{\omega}_1 \leq \bar{\omega} \leq$

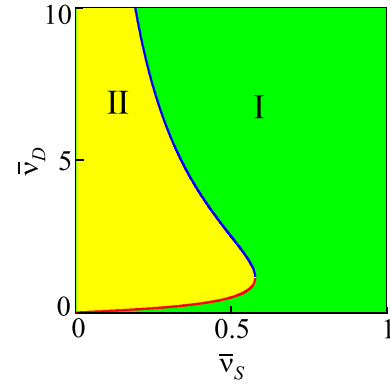


FIG. 4. Parameter space plot showing the boundary between two regions corresponding to scenarios I and II, for the case $a \gg 1$. Region I is in green, and region II is in yellow. The red curve stands for the function $\bar{\nu}_D^{(-)}(\bar{\nu}_S)$ and the blue curve represents the function $\bar{\nu}_D^{(+)}(\bar{\nu}_S)$.

$\bar{\omega}_2$ both branches coexist, closing at $\bar{\omega} = \bar{\omega}_2$. At the junction of two branches, we have $\bar{\omega} = \bar{\omega}_2$. If $a\bar{\nu}_0 \gg 1$ and $\bar{\nu}_0 \gg \bar{\nu}_1$, then $\bar{\omega}_2 \approx \sqrt{3}/3$. The angle $\theta_2 = \arcsin(\sqrt{3}/3) \approx 35^\circ$ corresponds to that frequency of rotation of the spiral. For $\bar{\omega} > \bar{\omega}_2$, Eq. (29) has no solutions in the region of acceptable values of the function $\bar{\omega}(\bar{\omega})$.

For exploring the implementation of scenario II, let us represent the formal condition (33) in terms of the parameters $\bar{\nu}_S$ and $\bar{\nu}_D$ instead of the parameters $\bar{\nu}_0$ and $\bar{\nu}_1$. The inequality $\Omega/\Omega_H \ll 1$ is assumed to be fulfilled for the helimagnets described. This allows one to put the parameter $\bar{\nu}_1$ in the form $\bar{\nu}_1 = \bar{\nu}_S + \bar{\nu}_D + 1/(\bar{\nu}_S + \bar{\nu}_D)$. Then, it can be shown that for the condition (33) to be satisfied, it is necessary that the following set of inequalities hold:

$$\bar{\nu}_S < \frac{1}{\sqrt{3} + 1/2a}, \quad (34)$$

$$\bar{\nu}_D^{(-)} < \bar{\nu}_D < \bar{\nu}_D^{(+)}, \quad (35)$$

where

$$\bar{\nu}_D^{(\pm)} = 1/\bar{\nu}_S - 1/2a \pm \sqrt{(1/\bar{\nu}_S - 1/2a)^2 - 3 - \bar{\nu}_S}. \quad (36)$$

According to (34), in order to implement scenario II, the parameter $\bar{\nu}_S$ should be sufficiently small. For the values of $\bar{\nu}_S \ll 1$, the condition (35) at $a \geq 1$ takes a simple form: $\bar{\nu}_S/2 < \bar{\nu}_D < 2/\bar{\nu}_S$.

Figure 4 displays a diagram of regions for the parameters $\bar{\nu}_S$ and $\bar{\nu}_D$ to implement conditions for scenarios I and II to be fulfilled.

A separate discussion is required for the question of the conditions for achieving the maximum possible rotation frequency of the magnetic spiral of the helimagnet, $\omega = \Omega$.

When the condition (30) is satisfied, this can be realized by gradually increasing the current passing through the helimagnet. The growth of the electron drift velocity and an appropriate increase in $\bar{\omega}$ from 0 to $\bar{\omega}_1$ are responsible for a monotonous increase in the spiral rotation frequency ω from 0 to Ω . In other words, the fulfillment of the condition (30) makes it possible to achieve the limiting rotation frequency

Ω by gradually increasing the current flowing through the helimagnet.

When the condition (33) is satisfied, a simple pattern of the monotonic increase in $\bar{\omega}$, as \bar{w} rises, remains only in the range of $0 \leq \bar{w} \leq \bar{w}_1$, where the mode $\bar{\omega}^{(1)}(\bar{w})$ is excited. Upon reaching \bar{w} the value \bar{w}_1 , the frequency of this mode amounts to the value $\bar{\omega}^{(1)}(\bar{w}_1)$ that is undoubtedly less than unity. Upon exceeding \bar{w} the value \bar{w}_1 , a situation takes place when the magnetic spiral can simultaneously be in two states with different rotational frequencies $\bar{\omega}^{(1)}(\bar{w})$ and $\bar{\omega}^{(2)}(\bar{w})$ at the identical value of \bar{w} . Such a situation can be observed in the range $\bar{w}_1 \leq \bar{w} \leq \bar{w}_2$. This phenomenon can be called current-induced spin rotation bistability of helimagnets.

The developed theory cannot predict which of these two excited states of the helimagnet's magnetic system rotating under action of electric current will be realized in the experiment. It can be assumed that current-density fluctuations existing in a real helimagnet, spatial inhomogeneities parameters of electron momentum and spin relaxation, and other random causes will lead to chaotic-in-time transitions between states with rotation frequencies $\bar{\omega}^{(1)}(\bar{w})$ and $\bar{\omega}^{(2)}(\bar{w})$. Such a "chaotic" regime does not enable the helimagnet's magnetic system to rotate stably with the maximum possible frequency $\omega = \Omega$. The bistability described above can also trigger hysteresis-type phenomena, as the magnitude of the electric current flowing through the helimagnet changes cyclically.

Whether the condition (30) is fulfilled or not, for the range $\bar{w} < 1$, using Eq. (29), we come up with its unique solution in the form

$$\bar{\omega} = \frac{1}{1 + a(\bar{v}_S + \bar{v}_D + 1/\bar{v}_S)} \bar{w}. \quad (37)$$

According to (37), the change in $\bar{\omega}$ with growth of \bar{w} is determined by three independent parameters a , \bar{v}_S , and \bar{v}_D . Let the values of the parameters a and \bar{v}_D be assigned. Then, we can treat Eq. (37) as an equation of a one-parameter family of functions $\bar{\omega} = \bar{\omega}(\bar{w}, \bar{v}_S)$. A unified characteristic of the entire one-parameter family of the functions $\bar{\omega}(\bar{w}, \bar{v}_S)$ is the discriminant curve $\bar{\omega}_d(\bar{w})$. In turn, the latter is a result of jointly solving the equations $\bar{\omega} - \bar{\omega}(\bar{w}, \bar{v}_S) = 0$ and $\partial \bar{\omega}(\bar{w}, \bar{v}_S) / \partial \bar{v}_S = 0$. The second equation has the solution $\bar{v}_S = 1$, and, consequently, the discriminant of Eq. (37) is written as

$$\bar{\omega}_d = \frac{1}{1 + a(2 + \bar{v}_D)} \bar{w}. \quad (38)$$

It is easy to see that the discriminant (38) yields the highest possible value of the function (37) for an arbitrary value of the parameter \bar{v}_S . In other words, the rotation frequency of the magnetic spiral of the helimagnet with arbitrary values of the parameters \bar{v}_S , \bar{v}_D , and a cannot exceed the value derived from formula (38).

To estimate the rotation frequency of a spin spiral in real helimagnets, as well as to verify approximations made on the pages of this paper, we need detailed information on the numerical values of all the parameters involved in the theory.

VI. NUMERICAL CALCULATIONS AND ESTIMATES

The theory we have built is directly and fully applicable to conductive helimagnets whose magnetic order obeys the Dzyaloshinskii-Moriya interaction. In the scientific literature for designating such helimagnets, the term "chiral helimagnets" and the appropriate abbreviation CHM are used [22]. As examples of such CHMs, we consider helimagnets FeGe, MnSi, and CrNb₃S₆. Characteristics of the Dzyaloshinskii-Moriya interaction determine the magnitude of parameters q_0 and B_F for CHM. Apart from CHM, there are magnets in which helimagnetism arises due to the exchange interaction, if exchange interaction between the nearest neighbors is positive while the exchange interaction between the next-nearest neighbors is negative. Among them are rare-earth metals Dy, Tb, Ho, Er, and Tm. Here, we consider Dy as an example. To describe helimagnets mentioned above, we resort to the findings secured for CHM provided that the characteristics q_0 and B_F as phenomenological parameters will be taken from experiment.

To numerically estimate the desired parameters, we exploit experimentally observed characteristics of FeGe, MnSi, CrNb₃S₆, and Dy helimagnets, contained in Table I. References to the sources of the given data are enclosed by square brackets.

The second column of the table includes data on the concentration N of conduction electrons in a helimagnetic crystal. The third column holds the values of the specific electrical resistivity ρ for the helimagnets. The fourth column contains data on the unit-cell volume V of the helimagnetic crystals. The fifth column lists the experimental values of the wave number q_0 of the magnetic spiral of the helimagnets. The sixth column shows the values of the magnetic field strength H_F directed along the axis of the magnetic spiral, upon reaching which the helimagnets pass into a ferromagnetic state. In the seventh column, one can find the values of the helimagnets' magnetization \mathcal{M}_F at the point of the above transition. The eighth column gives the values of the Gilbert damping constant α .

The values of the characteristics of each helimagnet being temperature dependent, the values of ρ , q_0 , \mathcal{M}_F , and H_F for all the helimagnets at hand correspond to those near the lowest temperature at which helimagnetism exists in them. In particular, the values of these quantities in the FeGe helimagnet are given for a temperature of 5 K, in MnSi—for a temperature of 4.2 K, in CrNb₃S₆—for a temperature of 2 K, and in Dy—for a temperature of 93.3 K.

We were unable to find any publication mentioning direct measurements of H_F for dysprosium. Therefore, the value of H_F for Dy specified in Table I is a result of the linear extrapolation of the data on the isothermal magnetization of Dy into the regions of strong magnetic fields [41].

Table I provides information on the value of the Gilbert damping constant α only for FeGe, for which $\alpha = 0.01$. For the other helimagnets described, no direct data could be found. For the Fe_{0.8}Co_{0.2}Si helimagnet, according to the data of Ref. [42], the magnitude of α amounts to 0.4 ± 0.1 . For numerical estimates of α , we will use values from the interval $\alpha \leq 1$.

TABLE I. Experimental data on the characteristics of FeGe, MnSi, CrNb₃S₆, and Dy metallic helimagnets.

Helimagnet	N (1/cm ³)	ρ ($\mu\Omega$ cm)	V (\AA^3)	q_0 (cm ⁻¹)	H_F (Oe)	\mathcal{M}_F (erg/G cm ³)	α
FeGe	2.4×10^{22} [23]	14 [24]	103.8 [25]	9.1×10^5 [26]	5.0×10^3 [24]	282 [24]	1×10^{-2} [27]
MnSi	6.3×10^{22} [28]	2 [29]	94.8 [30]	3.4×10^6 [31]	6.2×10^3 [32]	157 [32]	
CrNb ₃ S ₆	0.9×10^{21} [33]	60 [34]	398.3 [34]	1.3×10^6 [35]	2.0×10^4 [36]	147 [36]	
Dy	4.7×10^{22} [37]	38 [38]	72.9 [39]	1.7×10^7 [40]	2.8×10^5 [41]	2568 [41]	

The values of the electron concentration N given in Table I make it possible to quantify the characteristics of the system of conduction electrons. Let the electron gas be degenerate. For estimates in order of magnitude, we assume that the electron dispersion law is isotropic and quadratic, the effective mass of electrons is equal to the mass m_e of a free electron, and the value of the g factor is equal to 2. This simplest model suggests the Fermi energy of the gas of free electrons is $\varepsilon_F = \hbar^2(3\pi^2N)^{2/3}/2m_e$, the electron velocity on the Fermi surface is $v_F = (2\varepsilon_F/m_e)^{1/2}$, and the Pauli spin susceptibility is $\chi = 3N\mu_B^2/2\varepsilon_F$.

The calculated Fermi energy allows estimation of the dimensionless parameter Λ characterizing the degree of the s - d exchange interaction. For this, Λ can be represented as $\Lambda = IV/4\mu_B^2$, where I is the integral of the s - d exchange interaction, averaged over the unit-cell volume V . One of the authors of the s - d model offers a universal estimate for the exchange integral I [43]. According to the data, the value of I is determined by the Fermi energy magnitude ε_F and lies in the interval $(10^{-2}-10^{-1})\varepsilon_F$. To be definite, let us consider the lower limit of this estimate, setting $I = 0.01\varepsilon_F$.

Exploiting the Drude formula for the conductivity of an electron gas, we can estimate the relaxation time of the electron momentum, $\tau = m_e/\rho e^2N$. Knowing τ , it is not hard to evaluate the diffusion coefficient $D = v_F^2\tau/3$ and then the spin-diffusion relaxation rate, $\nu_D = q_0^2D$.

To compute the theory parameters Ω_H , Ω , and β we use the formulas $\Omega_H = \gamma\Lambda M$, $\Omega = \gamma(B_F + 4\pi M)$, and $\beta = 16\pi^2\gamma M/c^2q_0^2\rho$, in accordance with their definitions. The magnetization M appearing in these formulas is related to the experimentally determined quantity \mathcal{M}_F through $M = \mathcal{M}_F/(1 + \chi\Lambda)$. The magnetic field B_F is related to the experimentally measured strength H_F of the external magnetic field as $B_F = H_F + 4\pi\mathcal{M}_F$.

The values calculated in such a way for the susceptibility χ , the exchange interaction parameter Λ , the momentum relaxation time τ , the rate ν_D , the frequencies Ω_H and Ω , as well as for parameter β are summarized in Table II.

From Table II, it is seen that the quantity $\beta \sim 10^{-7}-10^{-6}$ is extremely small and, therefore, the cost accounting for radiation of electromagnetic waves by the helimagnets does not dramatically change the pattern of the decay of the magnetic spiral rotation.

The available literature lacks experimental data on the values of the spin-lattice relaxation rate ν_S in helimagnets.

Therefore, in further consideration, the quantity ν_S remains a free parameter of the theory.

For all the metallic helimagnets here considered (see Table II), the relations $\chi \ll 1$ and $\chi\Lambda \ll 1$, applied above for deriving the set of equations (14) and (15), are fulfilled. The strong inequality $\Omega/\Omega_H \ll 1$ we used for defining the conditions (34) and (35) also holds.

Let us illustrate the use of obtained equations for numerical calculation of $\bar{\omega}(\bar{w})$ for FeGe helimagnet. In this case, the values of the parameters a and $\bar{\nu}_D$ are $a \approx 1$ and $\bar{\nu}_D \approx 0.05$, respectively. Figure 5 shows the results of numerical solution of Eq. (29) for $\bar{\omega}(\bar{w})$ at fixed values of the parameters $a = 1$ and $\bar{\nu}_D = 0.05$ and for three different values of $\bar{\nu}_S$. For scenario II to be realized, the condition (35) should take the form $\bar{\nu}_S < 0.09$. Curve II in Fig. 5 is plotted for the value $\bar{\nu}_S = 0.05$ within the specified range. At $\bar{\nu}_S > 0.09$, scenario I is implemented. Curve I in Fig. 5 is built at the value $\bar{\nu}_S = 1$. The dashed curve plotted at $\bar{\nu}_S = 0.09$ is the boundary of the regions of existence of scenarios I and II.

Let us estimate the magnitude of \bar{w}_1 to implement scenario II. In our case, we have $\bar{w}_1 = 1 + a[\bar{\nu}_S + \bar{\nu}_D + 1/(\bar{\nu}_S + \bar{\nu}_D)]$. Obviously, $\bar{w}_1 \geq 1 + 2a$ for any values of $\bar{\nu}_S$ and $\bar{\nu}_D$. Con-

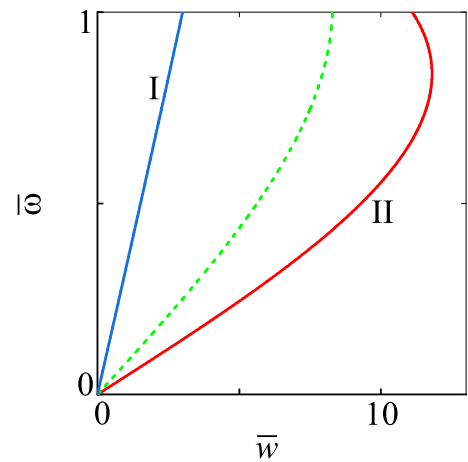


FIG. 5. Illustration of two scenarios of the behavior of the rotation frequency of the spin spiral with changing the drift velocity of electrons using FeGe as an example. Curve I: $\bar{\nu}_S = 1$, represents scenario I; curve II: $\bar{\nu}_S = 0.05$, represents scenario II; dashed curve: $\bar{\nu}_S = 0.09$, corresponds to the boundary of the regions of existence of scenarios I and II. For all three curves $a = 1$ and $\bar{\nu}_D = 0.05$.

TABLE II. Predicted values of the theory parameters for helimagnets FeGe, MnSi, CrNb₃S₆, Dy.

Helimagnet	χ	Λ	τ (s)	v_D (1/s)	Ω_H (1/s)	Ω (1/s)	β
FeGe	6.4×10^{-7}	1.5×10^4	1.2×10^{-15}	3.5×10^{12}	7.2×10^{13}	2.1×10^{11}	7.4×10^{-6}
MnSi	8.8×10^{-7}	2.5×10^4	3.1×10^{-15}	2.4×10^{14}	6.9×10^{13}	1.8×10^{11}	2.0×10^{-6}
CrNb ₃ S ₆	2.1×10^{-7}	6.3×10^3	7.3×10^{-15}	4.9×10^{12}	1.6×10^{13}	4.1×10^{11}	4.5×10^{-7}
Dy	8.0×10^{-7}	1.6×10^4	2.2×10^{-16}	3.5×10^{14}	7.2×10^{14}	6.0×10^{12}	7.1×10^{-8}

sequently, in any case, for the condition $\bar{w} = \bar{w}_1$ to be achieved, the drift velocity w should be larger than value $w_c = \Omega/q_0$, which corresponds to the electric current density $j_c = N|e|\Omega/q_0$. The calculated values of w_c and j_c are listed in Table III.

The obtained values of w_c and j_c are very large for all helimagnets under consideration. When currents with a density of (10^7-10^8) A/cm² flow in any metal conductor, a very significant Joule heat is produced, leading to the destruction of the sample. Therefore, the experimental implementation of scenario II in metallic helimagnets seems to be extremely difficult.

For density currents $j \ll j_c$ and $\bar{w} \ll 1$, the highest achievable value of the rotation frequency ω_d of the spin spiral can be determined by formula (38), as represented below:

$$\omega_d = \frac{1}{1 + (\alpha_{\text{eff}}/\chi\Lambda)(2 + v_D/\Omega_H)} \frac{q_0}{N|e|} j. \quad (39)$$

When the damping parameter α_{eff} is small compared to the product $\chi\Lambda$, from (39) we can come to a simple estimate $\omega_d = (q_0/N|e|)j$. The results of calculating the frequency ω_d and angle $\theta_d = \arcsin(\omega_d/\Omega)$ for various values of the damping parameter α are shown in Fig. 6. Figs. 6(a) and 6(c) include the $\omega_d(j)$ - and $\theta_d(j)$ dependencies for all the above helimagnets; the damping parameter is equal to $\alpha = 0.01$, which corresponds to FeGe. Figures 6(b) and 6(d) involve the same curves plotted for extremely small $\alpha \ll \chi\Lambda$, when $\omega_d \approx (q_0/N|e|)j$.

Estimations conducted demonstrate that in metallic helimagnets, the rotation frequency of the spin spiral can reach tens of gigahertz at a rotation-inducing current density of $j \leq 10^7$ A/cm². The rotation frequency at a given current-density value depends significantly on the parameter $a = \alpha_{\text{eff}}/\chi\Lambda$: the lower the damping parameter α , the greater the rotation frequency. In the case of extremely small values of the parameter α , the highest value of the rotation frequency ω_d is directly proportional to the wave number q_0 of the magnetic spiral. The conicity angle of the spiral does not exceed 10°.

From expression (25) it is easy to find the highest possible value of the Umov-Poynting vector. It can be seen that this value does not exceed the magnitude of $U_c = 4\pi M^2 \Omega^3 / c^2 q_0^3$. The values of U_c calculated by this formula are presented in the third column of Table III. For dysprosium, the value of U_c in order of magnitude reaches 10^{-4} W/cm².

It should be underscored that the results obtained for MnSi and FeGe are applicable for a qualitative description of the magnetic spiral rotation patterns in a large class of conductive cubic inversion-center-free magnets—in transition-metal silicides such as MnSi, Fe_{1-x}Co_xSi, Mn_{1-x}Fe_xSi, Mn_{1-x}Co_xSi and in FeGe, MnGe, Mn_{1-x}Fe_xGe, Fe_{1-x}Co_xGe transition-metal germanides.

VII. CONCLUSIONS

As a result of the investigation of the spin dynamics of conductive chiral helimagnets, based on simultaneous solution of the Bloch-Torrey equation for the magnetization of itinerant electrons, the Landau-Lifshitz-Gilbert equation for the magnetization of localized electrons, and Maxwell's equations for an electromagnetic field, we can note the following peculiarities of spin-torque transfer from the spin system of conduction electrons to that of localized electrons:

1. A constant flow of electrons (with a uniform time rate) along the chiral helimagnet axis with a drift velocity \mathbf{w} , due to the STT effect, induces the rotation of the magnetic spiral of the helimagnet with an angular frequency ω . The ω -frequency sign that specifies the direction of rotation of the spiral with a wave vector \mathbf{q} is determined by the sign of the scalar product $(\mathbf{q} \cdot \mathbf{w})$. The magnitude of the frequency depends on the ratio of the Gilbert damping parameter and a parameter characterizing the efficiency of the SST processes. The latter is governed by the magnitude of the constant of the exchange interaction between conduction and localized electrons. For helimagnets with extremely low Gilbert damping, the frequency ω , with an accuracy of a numerical factor of the order of unity, is equal to $(\mathbf{q} \cdot \mathbf{w})$. All the quantities used in our theoretical model are

TABLE III. Estimates for the quantities w_c , j_c , and U_c .

Helimagnet	w_c (cm/s)	j_c (A/cm ²)	U_c (W/cm ²)
FeGe	2.3×10^5	8.8×10^8	1.4×10^{-6}
MnSi	5.3×10^4	8.6×10^8	4.7×10^{-9}
CrNb ₃ S ₆	3.1×10^5	4.5×10^7	1.0×10^{-6}
Dy	3.5×10^5	2.6×10^9	3.9×10^{-4}

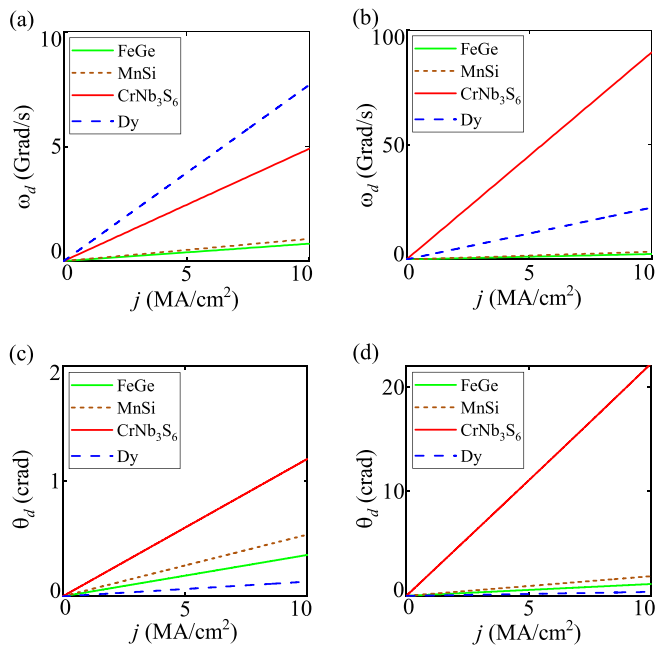


FIG. 6. The highest values of the rotation frequency ω_d for the spin spiral (a), (b) and conicity angle θ_d (c), (d) for metallic helimagnets FeGe, MnSi, CrNb₃S₆, Dy: (a), (c) $\alpha = 0.01$; (b), (d) $\alpha \ll \chi \Lambda$.

expressed in terms of the quantum-exchange Hamiltonian that produces helical magnetic ordering in conductive crystals.

2. The STT effect leads to the fact that the wavelength of the helimagnet's magnetic spiral rotating under the flowing spin current is always slightly smaller than that of the stationary magnetic spiral. The spin current also influences conicity of the magnetic helicoid. The angle θ characterizing the conicity augments with increasing the frequency of rotation of the magnetic spiral.

3. It is found that the Poynting vector that sets the direction of propagation of the electromagnetic field energy generated by an electric current flowing in a chiral helimagnet is directed along the vector of the conduction electron flux, regardless of the helimagnet chirality. In calculating the rotation frequency of the magnetic spiral, accounting for the generation of an electromagnetic field, is reduced to an effective increase in the Gilbert damping parameter and an increase in the limiting rotation frequency of the spiral.

The authors hope that the present study has a considerable potential for inspiring future in-depth research of chiral conductive helimagnets that may eventually lead to the development of functional components for spintronic devices: spin generators converting direct electric current into high-frequency electromagnetic field, and spin diodes performing the inverse conversion.

ACKNOWLEDGMENT

This research has been carried out under the financial support of the Russian Science Foundation within the framework of Project No. 22-22-00220.

- [1] J. C. Slonczewski, Current-driven excitation of magnetic multilayers, *J. Magn. Magn. Mater.* **159**, L1 (1996).
- [2] L. Berger, Emission of spin waves by a magnetic multilayer traversed by a current, *Phys. Rev. B* **54**, 9353 (1996).
- [3] L. Berger, Multilayers as spin-wave emitting diodes, *J. Appl. Phys.* **81**, 4880 (1997).
- [4] L. Berger, Spin-wave emitting diodes and spin diffusion in magnetic multilayers, *IEEE Trans. Magn.* **34**, 3837 (1998).
- [5] M. Tsoi, A. G. M. Jansen, J. Bass, W.-C. Chiang, M. Seck, V. Tsoi, and P. Wyder, Excitation of a Magnetic Multilayer by an Electric Current, *Phys. Rev. Lett.* **80**, 4281 (1998).
- [6] J. A. Katine, F. J. Albert, R. A. Buhrman, E. B. Myers, and D. C. Ralph, Current-Driven Magnetization Reversal and Spin-Wave Excitations in Co/Cu/Co Pillars, *Phys. Rev. Lett.* **84**, 3149 (2000).
- [7] S. I. Kiselev, J. C. Sankey, I. N. Krivorotov, N. C. Emley, R. J. Schoelkopf, R. A. Buhrman, and D. C. Ralph, Microwave oscillations of a nanomagnet driven by a spin-polarized current, *Nature (London)* **425**, 380 (2003).
- [8] W. H. Rippard, M. R. Pufall, S. Kaka, S. E. Russek, and T. J. Silva, Direct-Current Induced Dynamics in Co₉₀Fe₁₀/Ni₈₀Fe₂₀ Point Contacts, *Phys. Rev. Lett.* **92**, 027201 (2004).
- [9] S. Mangin, D. Ravelosona, J. A. Katine, M. J. Carey, B. D. Terris, and E. E. Fullerton, Current-induced magnetization reversal in nanopillars with perpendicular anisotropy, *Nat. Mater.* **5**, 210 (2006).
- [10] T. Ono and Y. Nakatani, Magnetic domain wall oscillator, *Appl. Phys. Express* **1**, 061301 (2008).
- [11] A. Yamaguchi, T. Ono, S. Nasu, K. Miyake, K. Mibu, and T. Shinjo, Real-Space Observation of Current-Driven Domain Wall Motion in Submicron Magnetic Wires, *Phys. Rev. Lett.* **92**, 077205 (2004).
- [12] K. Goto, H. Katsura, and N. Nagaosa, Current-induced dynamics of spiral magnet, [arXiv:0807.2901](https://arxiv.org/abs/0807.2901).
- [13] S. K. Kudtarkar, Dynamics of helimagnets with spin polarised currents, *Phys. Lett. A* **374**, 366 (2009).
- [14] J. Iwasaki, M. Mochizuki, and N. Nagaosa, Universal current-velocity relation of skyrmion motion in chiral magnets, *Nat. Commun.* **4**, 1463 (2013).
- [15] K. M. D. Hals and A. Brataas, Spin-transfer torques in helimagnets, *Phys. Rev. B* **87**, 174409 (2013).
- [16] O. Wessely, B. Skubic, and L. Nordström, Current Driven Magnetization Dynamics in Helical Spin Density Waves, *Phys. Rev. Lett.* **96**, 256601 (2006).
- [17] J. Masell, X. Yu, N. Kanazawa, Y. Tokura, and N. Nagaosa, Combining the helical phase of chiral magnets with electric currents, *Phys. Rev. B* **102**, 180402(R) (2020).
- [18] Y. Takeuchi, Y. Yamane, J. Yoon, R. Itoh, B. Jinnai, S. Kanai, J. Ieda, S. Fukami, and H. Ohno, Chiral-spin rotation of non-collinear antiferromagnet by spin-orbit torque, *Nat. Mater.* **20**, 1364 (2021).

- [19] W. Gerlach and O. Stern, Der experimentelle nachweis der richtungsquantelung im magnetfeld, *Z. Phys.* **9**, 349 (1922).
- [20] V. V. Ustinov and I. A. Yasyulevich, Electron spin current and spin-dependent galvanomagnetic phenomena in metals, *Phys. Met. Metallogr.* **121**, 223 (2020).
- [21] V. V. Ustinov and I. A. Yasyulevich, Electrical magnetochiral effect and kinetic magnetoelectric effect induced by chiral exchange field in helical magnetics, *Phys. Rev. B* **102**, 134431 (2020).
- [22] J. Kishine and A. S. Ovchinnikov, Theory of monoaxial chiral helimagnet, *Solid State Phys.* **66**, 1 (2015).
- [23] N. A. Porter, J. C. Gartside, and C. H. Marrows, Scattering mechanisms in textured FeGe thin films: Magnetoresistance and the anomalous Hall effect, *Phys. Rev. B* **90**, 024403 (2014).
- [24] J. F. DiTusa, S. B. Zhang, K. Yamaura, Y. Xiong, J. C. Prestigiacomo, B. W. Fulfer, P. W. Adams, M. I. Brickson, D. A. Browne, C. Capan, Z. Fisk, and J. Y. Chan, Magnetic, thermodynamic, and electrical transport properties of the non-centrosymmetric B20 germanides MnGe and CoGe, *Phys. Rev. B* **90**, 144404 (2014).
- [25] B. Lebech, J. Bernhard, and T. Freltoft, Magnetic structures of cubic FeGe studied by small-angle neutron scattering, *J. Phys.: Condens. Matter* **1**, 6105 (1989).
- [26] S.-A. Siegfried, A. S. Sukhanov, E. V. Altyntbaev, D. Honecker, A. Heinemann, A. V. Tsvyashchenko, and S. V. Grigoriev, Spin-wave dynamics in the helimagnet FeGe studied by small-angle neutron scattering, *Phys. Rev. B* **95**, 134415 (2017).
- [27] S. Budhathoki, A. Sapkota, K. M. Law, S. Ranjit, B. Nepal, B. D. Hoskins, A. S. Thind, A. Y. Borisevich, M. E. Jamer, T. J. Anderson, A. D. Koehler, K. D. Hobart, G. M. Stephen, D. Heiman, T. Mewes, R. Mishra, J. C. Gallagher, and A. J. Hauser, Room-temperature skyrmions in strain-engineered FeGe thin films, *Phys. Rev. B* **101**, 220405(R) (2020).
- [28] V. V. Glushkov, I. I. Lobanova, V. Yu. Ivanov, and S. V. Demishev, Anomalous Hall effect in MnSi: Intrinsic to extrinsic crossover, *JETP Lett.* **101**, 459 (2015).
- [29] K. Kadowaki, K. Okuda, and M. Date, Magnetization and magnetoresistance of MnSi. I, *J. Phys. Soc. Jpn.* **51**, 2433 (1982).
- [30] S. M. Stishov and A. E. Petrova, Itinerant helimagnet MnSi, *Phys.-Usp.* **54**, 1117 (2011).
- [31] S. V. Grigoriev, S. V. Maleyev, A. I. Okorokov, Y. O. Chetverikov, P. Böni, R. Georgii, D. Lamago, H. Eckerlebe, and K. Pranzas, Magnetic structure of MnSi under an applied field probed by polarized small-angle neutron scattering, *Phys. Rev. B* **74**, 214414 (2006).
- [32] M. K. Chattopadhyay, P. Arora, and S. B. Roy, Magnetic properties of the field-induced ferromagnetic state in MnSi, *J. Phys.: Condens. Matter* **21**, 296003 (2009).
- [33] A. C. Bornstein, B. J. Chapman, N. J. Ghimire, D. G. Mandrus, D. S. Parker, and M. Lee, Out-of-plane spin-orientation dependent magnetotransport properties in the anisotropic helimagnet Cr_{1/3}NbS₂, *Phys. Rev. B* **91**, 184401 (2015).
- [34] X. Li, Z. Li, H. Li, Y. Yao, X. Xi, Y.-C. Lau, and W. Wang, Angular-dependent magnetoresistance in Cr_{1/3}NbS₂ single crystals, *Appl. Phys. Lett.* **120**, 112408 (2022).
- [35] Y. Cao, Z. Huang, Y. Yin, H. Xie, B. Liu, W. Wang, C. Zhu, D. Mandrus, L. Wang, and W. Huang, Overview and advances in a layered chiral helimagnet Cr_{1/3}NbS₂, *Mater. Today Adv.* **7**, 100080 (2020).
- [36] T. Miyadai, K. Kikuchi, H. Kondo, S. Sakka, M. Arai, and Y. Ishikawa, Magnetic properties of Cr_{1/3}NbS₂, *J. Phys. Soc. Jpn.* **52**, 1394 (1983).
- [37] C. J. Kevane, S. Legvold, and F. H. Spedding, The Hall effect in yttrium, lanthanum, cerium, praseodymium, neodymium, gadolinium, dysprosium, and erbium, *Phys. Rev.* **91**, 1372 (1953).
- [38] P. M. Hall, S. Legvold, and F. H. Spedding, Electrical resistivity of dysprosium single crystals, *Phys. Rev.* **117**, 971 (1960).
- [39] J. Jensen and A. R. Mackintosh, *Rare Earth Magnetism* (Clarendon Press, Oxford, 1991).
- [40] J. Yu, P. R. LeClair, G. J. Mankey, J. L. Robertson, M. L. Crow, and W. Tian, Exploring the magnetic phase diagram of dysprosium with neutron diffraction, *Phys. Rev. B* **91**, 014404 (2015).
- [41] A. S. Chernyshov, A. O. Tsokol, A. M. Tishin, K. A. Gschneidner, Jr., and V. K. Pecharsky, Magnetic and magnetocaloric properties and the magnetic phase diagram of single-crystal dysprosium, *Phys. Rev. B* **71**, 184410 (2005).
- [42] J. D. Koralek, D. Meier, J. P. Hinton, A. Bauer, S. A. Parameswaran, A. Vishwanath, R. Ramesh, R. W. Schoenlein, C. Pfleiderer, and J. Orenstein, Observation of Coherent Helimagnons and Gilbert Damping in an Itinerant Magnet, *Phys. Rev. Lett.* **109**, 247204 (2012).
- [43] S. V. Vonsovskii, *Magnetism* (John Wiley & Sons, New York, 1974).